Technical Sciences
Academy of Romania
www.jesi.astr.ro

Journal of Engineering Sciences and Innovation
Volume 7, Issue 2 / 2022, pp. 131 - 142
http://doi.org/10.56958/jesi.2022.7.2.131

A. Mechanical Engineering

Received ***15 February 2022*** *Accepted* ***14 June 2022***
Received in revised form ***27 Apryl 2022***

Assessing mode indicator functions used in modal testing

MIRCEA RADEŞ*

Politehnica University of Bucharest, Splaiul Independenţei 313, Bucharest, Romania

Abstract. This paper presents a comparative study of the performance of some Mode Indicator Functions used in the modal testing of a structure with close modes, based on a restricted and non-optimal data set with a single reference. Best results are obtained using multi-curve modal indicators having the form of orthogonal projectors defined somewhat complementary to componentwise power spectra.

Keywords: Mode Indicator Functions, MIF, AMIF, QRMIF, CoMIF, QCoMIF.

1. Introduction

Mode Indicator Functions (MIFs) are real-valued frequency-dependent scalars that exhibit peaks or troughs at the modal frequencies of a structure. They are calculated using (measured) complex Frequency Response Functions (FRFs) to estimate the number of resonant modes that should be considered in the analysis.
Single-curve MIFs have been first developed [1] to isolate modes by sine dwell methods. They are efficient in the modal testing of structures with relatively low modal density and cannot reveal the existence of double modes.
Multi-curve MIFs have been used in applications with multi-input testing techniques. There are two categories in current use. In a first group, single frequency FRF (sub)-matrices are subjected in turn to either a Singular Value Decomposition (SVD) or an eigenvalue analysis. A full discussion of the performance of these MIFs can be found in [2].
A second category of MIFs work on Composite FRF matrices (CFRF) encompassing all available FRFs. When measured at N_o response coordinates, N_i input coordinates and N_f discrete frequencies, their size is $N_f \times N_o N_i$. The columns of the CFRF matrix contain the values for each response/reference combination at all N_f frequencies. The CFRF matrix is subjected to an SVD, QR or

*Correspondence address: mircearades@gmail.com

QLP decomposition. MIFs are plots of the left singular vectors or the q-vectors versus frequency. A comparison of the performance of these MIFs is made in [3].
Generally, it is considered that the only way that double or repeated modes can be detected is by using data from more than one reference. For structures exhibiting double modes, a common approach is to use additional masses. MIFs in the second category work well for such de-symmetrized structures even with single-reference data. In all cases one should be aware of the limitations of measured data, i.e. the insufficient information due to low spatial and frequency resolution.
This paper compares the performance of several MIFs in the case of measurements made at a reduced set of degrees of freedom and use of only one reference point, for a structure with a cluster of four modes.

2. Tested structure

The measurement data used in this paper were supplied by the Centre of Vibration Engineering at Imperial College, London, from modal tests on a twin of the original GARTEUR aircraft model, modified by a mass added to the tail [4].
The tested structure made of aluminum had a fuselage length of $1.5\ m$ and a wing span of $2\ m$ (Fig.1). The fuselage had a $50 \times 150\ mm$ rectangular cross section. The upper part of the tail and the two "drums" at the ends of the wing were $100 \times 400\ mm$. The total mass was $44\ kg$ and the mass added to the tail was $0.95\ kg$. Realistic damping levels were achieved by bonding a viscoelastic tape to the upper surface of the wing, covered by a thin aluminum constraining layer.

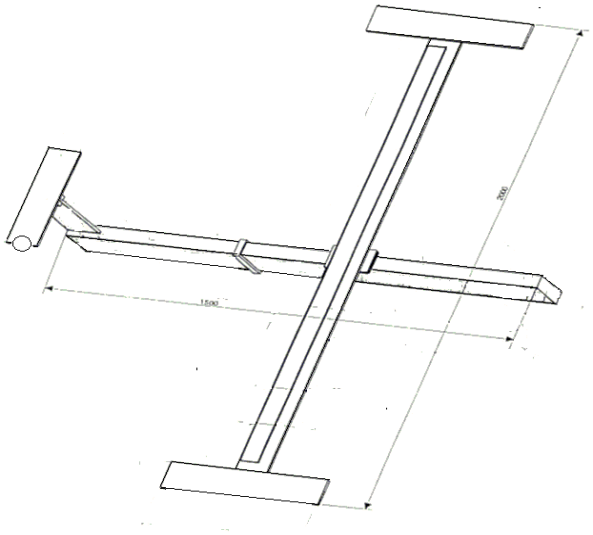

Fig. 1. Tested structure.

The structure was suspended using soft bungees. An accelerometer was attached in turn at each of the 24 degrees of freedom (DOFs) shown in Fig.2. The force gauge was attached to the underside of the wing, at DOF $12z$.

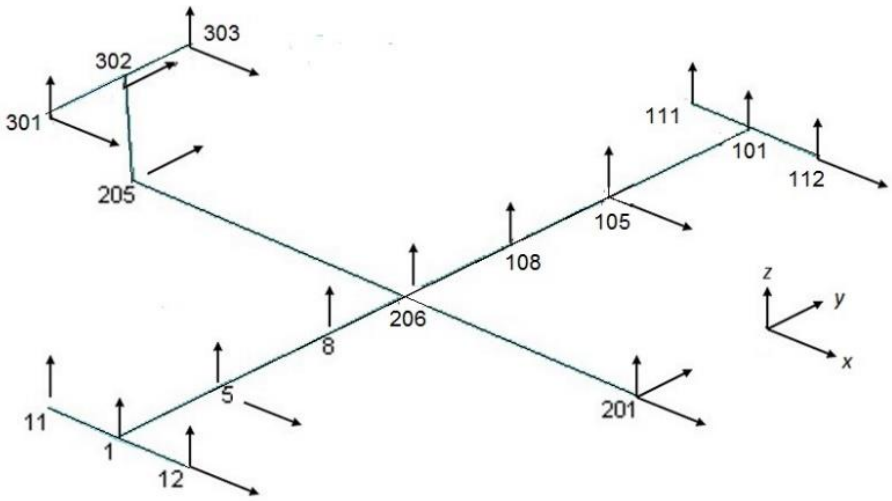

Fig. 2. Location and directions of test coordinates.

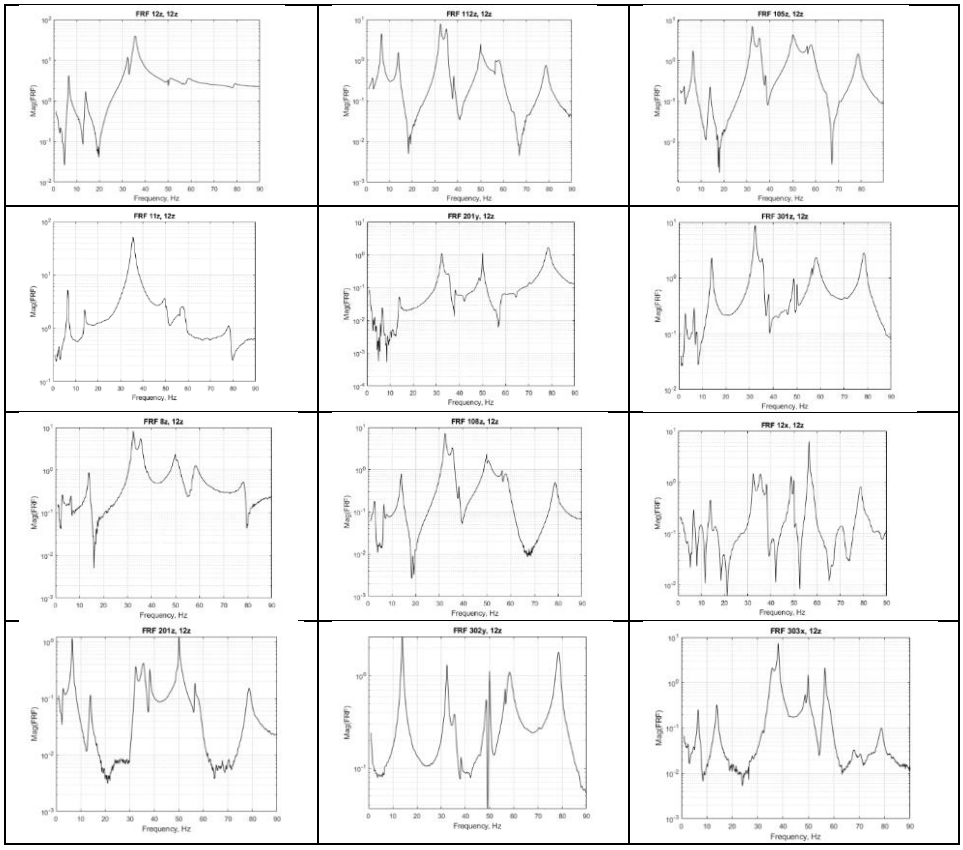

Fig. 3a. FRF curves.

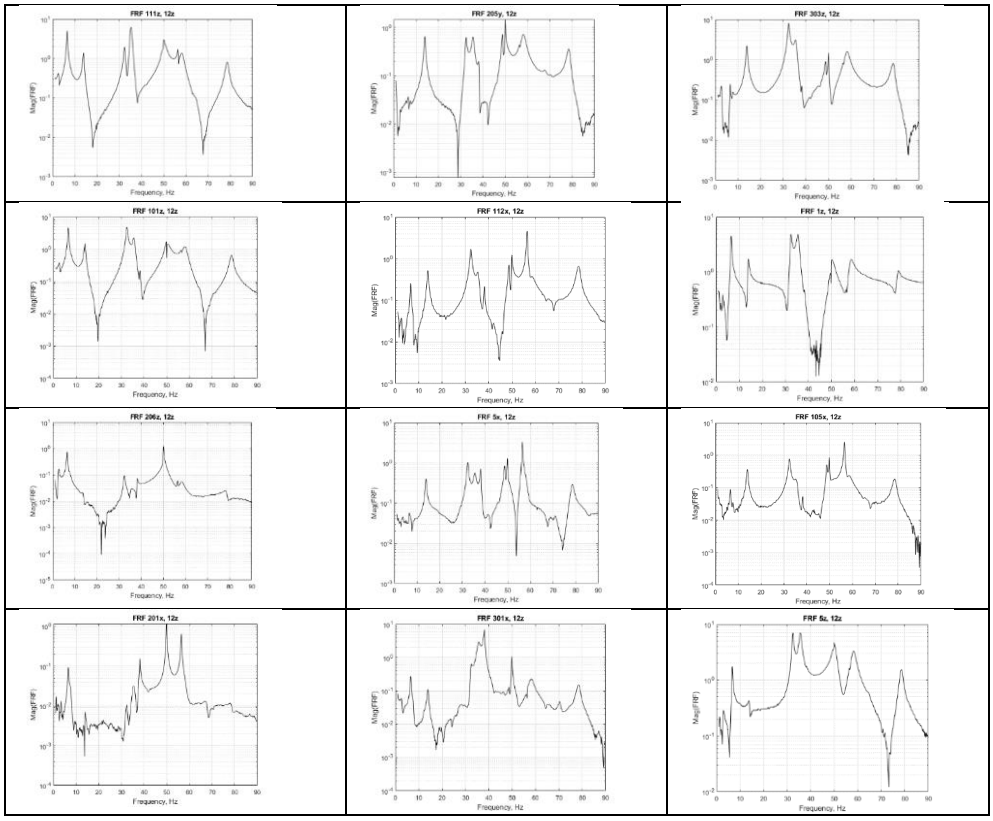

Fig. 3b. FRF curves.

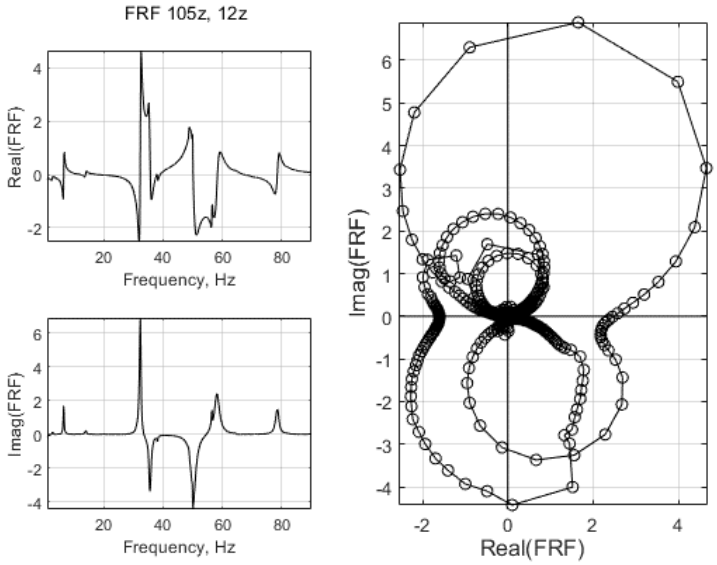

Fig. 4. Plots of a complex FRF.

3. FRF measurements

The experimental data-base, supplied in universal file format, consists of 24 complex-valued FRFs measured in the range 0 to100 Hz with a resolution of 0.125 Hz, using one hitting point at the right wing tip.
Receptance frequency response functions $FRFjk$, for displacement at coordinate j produced by excitation at coordinate k, are represented as magnitude (log scale) versus frequency (linear scale) plots in Fig.3, in the range 0-90 Hz. Figure 4 presents plots of the real and imaginary parts and the Nyquist plot of a typical FRF. The imaginary part of the FRF appears to be a good substitute for the complex value to pinpoint the resonance frequencies.

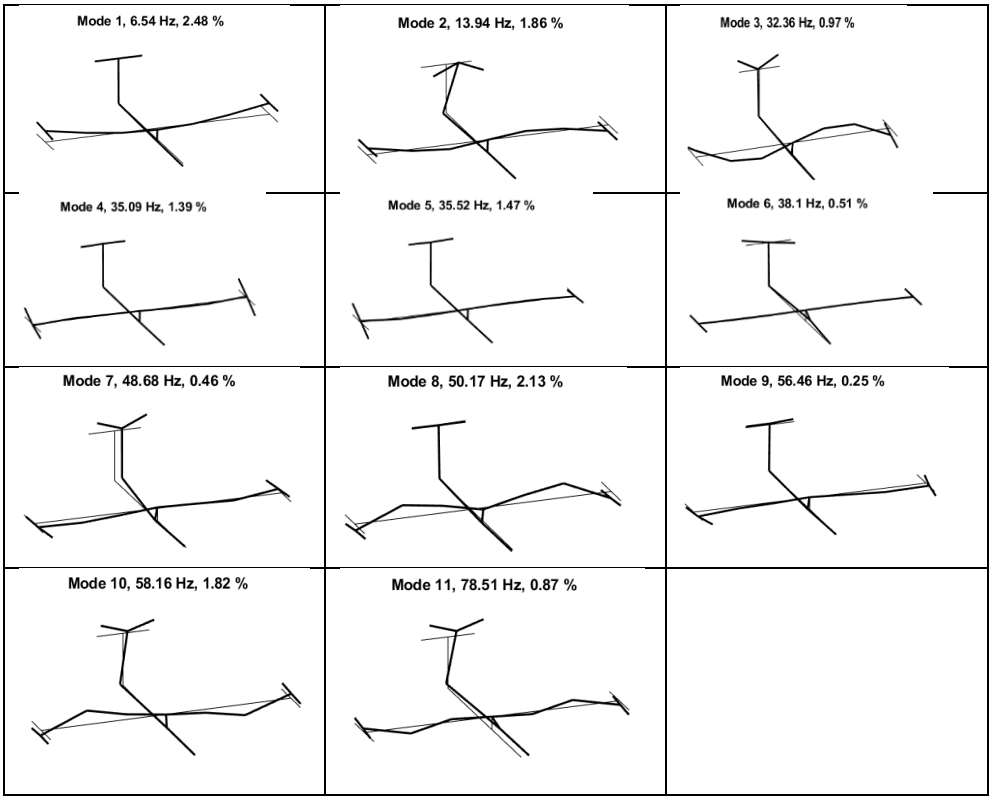

Fig.5. First 11 mode shapes

4. Natural frequencies and mode shapes

The first eleven modal shapes of the tested structure are shown in Fig.5.
The damped natural frequencies and modal damping ratios, calculated using the Global M parameter extraction method provided in the MODENT software are given in Table 1 [5].

The structure exhibits four close modes in the frequency range 32-36 Hz, two close modes between 48 and 50.2 Hz, and other two close modes between 56 and 58.2 Hz.
The wing first symmetric and antisymmetric torsion modes at 35.09 and 35.52 Hz have a very small relative frequency separation (1.2%) which, for a moderate damping ratio of 1.4%, makes the two resonances not individually discernable on FRF plots. They represent a double mode, split by the added mass which de-symmetrizes the structure.

Table 1. Modal parameters of tested structure.

Mode	Natural frequency, Hz	Damping ratio, %	Description
1	6.54	2.48	wing 2N bending
2	13.94	1.86	fuselage rotation
3	32.36	0.97	wing 3N bending
4	35.09	1.39	first symmetric wing torsion
5	35.52	1.47	first antisymmetric wing torsion
6	38.1	0.51	tail torsion
7	48.68	0.46	in-plane wing vs. fuselage
8	50.17	2.13	wing 4N bending
9	56.46	0.25	symmetric in-plane bending
10	58.16	1.82	second fuselage rotation
11	78.51	0.87	wing 5N bending

The aim of this paper is to document the ability of available MIFs to locate these close modes, showing their individual limitations as to accuracy and applicability to an actual structure.

5. Single curve MIFs

Most MIFs are intended for sets of FRF data from multiple references. However, several single curve MIFs have been developed based on a set of FRFs with a single reference.
Let $A = [a_{ij}]$ be the CFRF matrix of size $N_f \times N_o$, where $N_f = 721$ and $N_o = 24$.
At each frequency, using FRFs instead of displacement amplitudes, the DFVLR MIF [6] is defined as

$$MIF_i = 1 - \frac{\sum_{j=1}^{N_o} |Re(a_{ij})|\,|a_{ij}|}{\sum_{j=1}^{N_o} |a_{ij}|^2} \qquad (1)$$

where a_{ij} is the FRF measured at the output coordinate j and frequency i.
The MIF plot is shown in Fig.6a. The peaks in this plot locate the frequencies where the forced response is closest to the monophase condition. It provides no information concerning the modal response magnitudes.

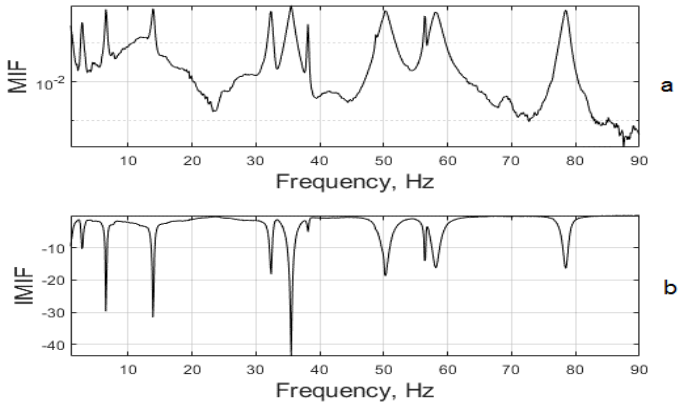

Fig. 6. MIF and IMIF plots.

An alternative mode indicator function (Fig.6b), defined by

$$IMIF_i = 1 - \frac{\sum_{j=1}^{N_o} |Im(a_{ij})|\,|a_{ij}|}{\sum_{j=1}^{N_o} |a_{ij}|^2}, \qquad (2)$$

has been historically used in force appropriation studies [7].

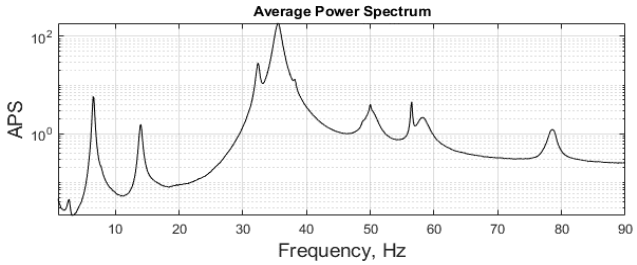

Fig. 7. APS plot.

The average power spectrum (APS) was defined as [8]

$$APS_i = \frac{\sum_{j=1}^{N_o} |a_{ij}|^2}{N_o}. \qquad (3)$$

It displays peaks at the resonance frequencies (Fig.7). The APS shows the relative magnitude of each modal response. Modes 6 and 7 are barely discernible.

An overlay of all 24 FRFs is depicted in Fig.8a. The plot of the sum of the magnitudes of all FRFs is given in Fig.8b, which resembles Fig.7.

Instead of directly using the FRFs, other single-curve MIFs have been developed based on combinations of FRFs, like the left singular vectors or the *q*-vectors from the pivoted QLR decomposition of the CFRF matrix.

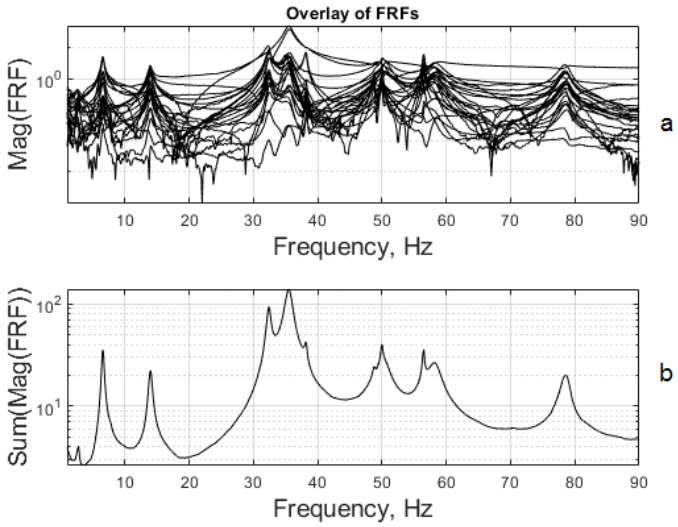

Fig. 8. Overlay and sum of FRF magnitudes.

In the basic formulation [9], the *Aggregate Mode Indicator Function* (AMIF) was defined as a vector containing the diagonal elements of the orthogonal projector onto the range of the CFRF matrix. If A is rank-deficient and its effective rank is N_r, then the AMIF is the vector of the diagonal elements of the orthogonal projector onto the subspace of left singular vectors

$$AMIF = diag(AA^{+}) = diag\left(\sum_{i=1}^{N_r} u_i u_i^{H}\right), \qquad (4)$$

where + denotes the pseudoinverse, u_i are left singular vectors and H denotes the conjugate transpose.

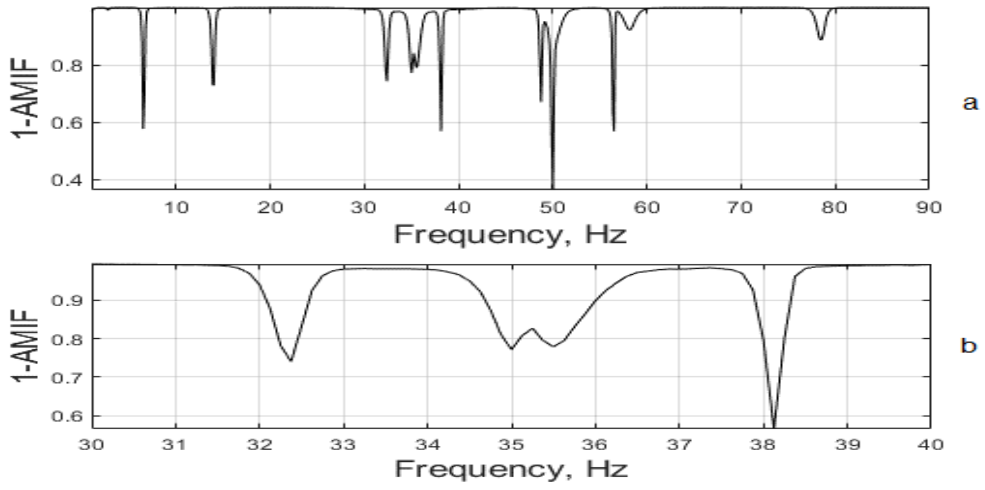

Fig. 9. Plots of 1-AMIF.

A more efficient mode indicator can be derived from its complement 1-AMIF, based on the orthogonal projector onto the null space of A^H. Figure 9a presents the 1-AMIF plot for an effective rank $N_r = 14$ of the imaginary part of the CFRF matrix. Figure 9b shows the 1-AMIF plot for the frequency range 30 to 40 Hz. All four modes in the cluster between 30 and 40 Hz are clearly highlighted.

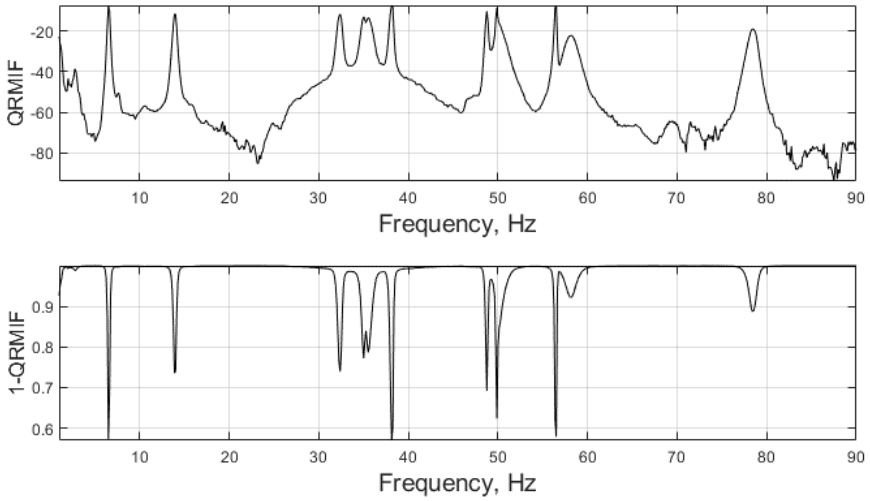

Fig. 10. Plots of QRMIF and 1-QRMIF.

The *QR Mode Indicator Function* (QRMIF) is an aggregate indicator based on the frequency dependence of the q-vectors obtained from the pivoted QR decomposition of the CFRF matrix [10]

$$QRMIF = diag\left(\sum_{i=1}^{N_r} q_i q_i^H\right). \quad (5)$$

The orthogonal q-vectors are combinations of the original measured FRFs. The QRMIF plot is almost identical to the AMIF plot when computed for the correct effective rank N_r. Plots of QRMIF and 1-QRMIF based on the imaginary part of the CFRF matrix are presented in Fig.10. They locate all eleven modes.

The MIF and IMIF plots fail to locate mode 7 at about 49 Hz and the quasi-double mode at about 35 Hz. In contrast, modes 5 and 7 are clearly indicated in the QRMIF plots and in the AMIF plot calculated for the imaginary part of the CFRF matrix (not shown here).

6. Multi curve MIFs

Multi-curve MIFs, based on the frequency-by-frequency analysis of FRF matrices, like the CMIF [11] and MMIF [12], are **not** considered herein. The present comparison is made for single input data, as measured on the modified GARTEUR testbed. Calculated for a single input, they resemble the MIF and IMIF plots.

To reveal the presence of very close modes, a multi-curve MIF has to be developed, based on some manipulation of the available FRFs.

The *Componentwise Mode Indicator Function* (CoMIF) is defined [13] by vectors of the form

$$CoMIF_j = diag\left(I_{N_f} - u_j u_j^H\right) = \mathbf{1} - u_j \otimes u_j^*, \qquad (6)$$

where I_{N_f} is the identity matrix of order N_f , u_j are left singular vectors of the CFRF matrix, **1** is a column vector of ones, $\otimes$ denotes elementwise multiplication, and the star superscript denotes the complex conjugate.

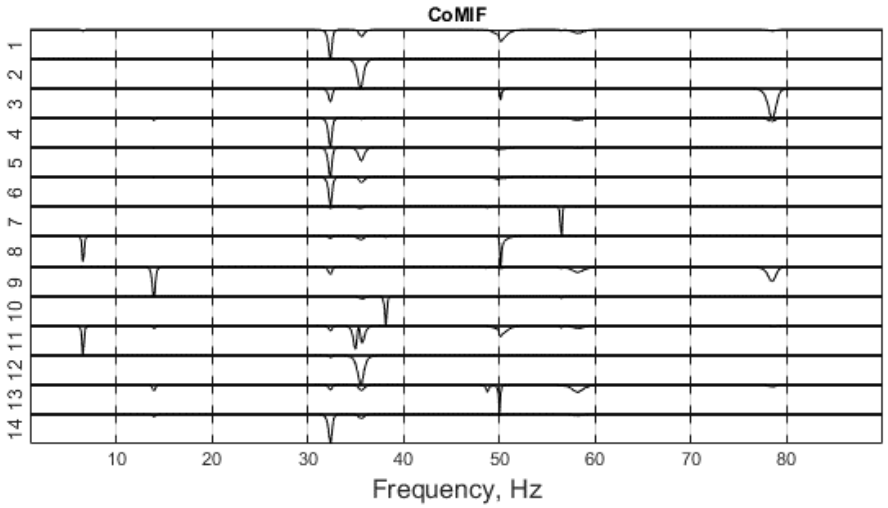

Fig. 11. CoMIF plot.

In the CoMIF plot (Fig.11), calculated using the imaginary part of the CFRF matrix, the number of subplots is equal to the effective rank of this matrix, $N_r = 14$, estimated from the decrease of its singular values (Fig.12).

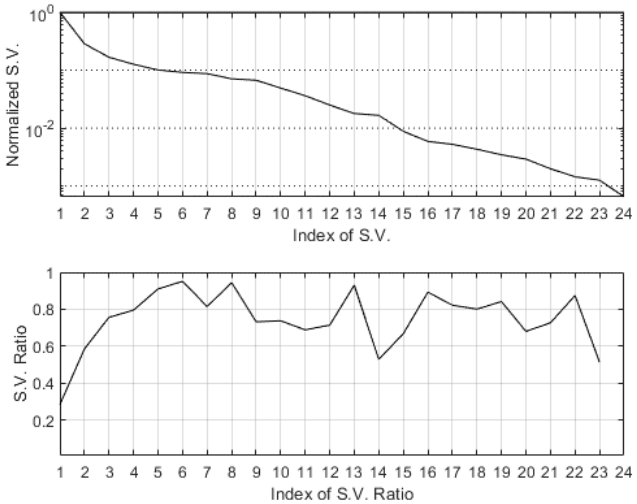

Fig. 12. Singular values plots.

Generally, each curve has local minima at the damped natural frequencies, with the deepest trough at the natural frequency of the corresponding dominant mode. The CoMIF plot in Fig.11 locates all eleven modes and outperforms the MIFs which fail to indicate one mode in the cluster of four modes at about 35 Hz.

The same information can be obtained by directly using the imaginary part of FRF vectors (squared to express power) instead of the left singular vectors. The main drawback is the arbitrary selection of the number of subplots.

Another MIF based on linear combinations of FRFs is the *Q-Vectors Componentwise Mode Indicator Function* (QCoMIF). It is constructed [10] using, instead of left singular vectors, *q*-vectors obtained from the QLP decomposition with column pivoting of the imaginary part of the measured complex CFRF matrix. It is defined by vectors of the form

$$QCoMIF_j = \mathbf{1} - q_j \otimes q_j^{*}. \qquad (8)$$

where q_j, called *Q*-Response Functions, are linear combinations of the measured FRFs. They are orthogonal, hence independent.

The QCoMIF plot (Fig.13) has as many curves (subplots) as the rank of the matrix in which the complex-valued FRFs have been replaced by their imaginary part. The rank is estimated from the decrease of the diagonal elements of the *L* matrix, which is similar to the decrease of the singular values.

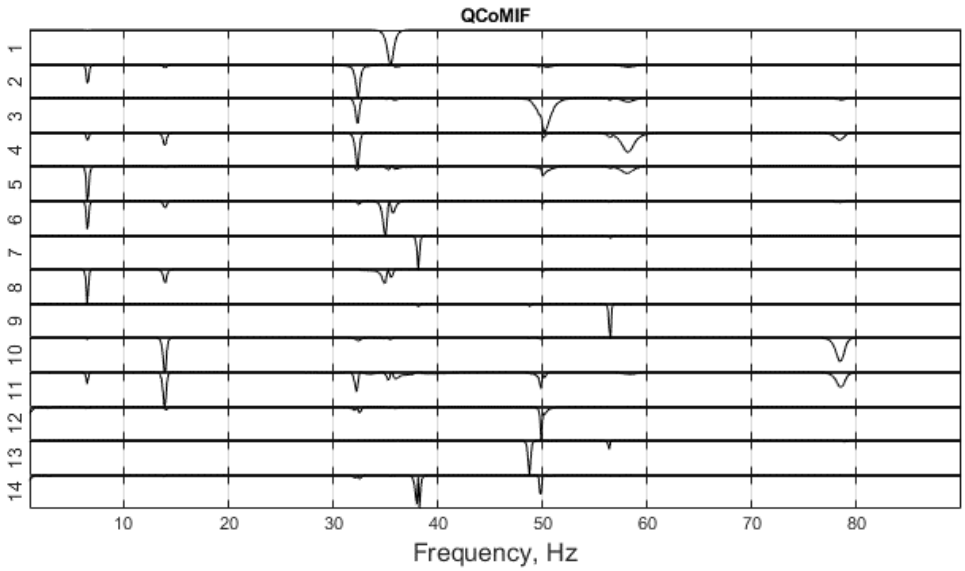

Fig. 13. QCoMIF plot.

The QCoMIF locates all eleven modes in the frequency range of measurements, including mode 5 at 35.5 Hz and mode 7 at about 48.7 Hz.

8. Concluding remarks

The aim of this paper was to assess the performance of some mode indicator functions in the analysis of single reference test data, arbitrary selection of a reduced number of response coordinates, and relatively low frequency resolution. Using actual measured test data, for a structure de-symmetrized by an additional mass, best results have been obtained with multi-curve MIFs based on the SVD or the pivoted QLP decomposition of a compound matrix encompassing the imaginary parts of all measured FRFs. The CoMIF and QCoMIF with separate subplots are able to detect the presence of very close modes.

References

[1] Breitbach E.J., *Recent developments in multiple input modal analysis*, J. of Vibration, Stress and Reliability in Design, vol.110, Oct 1988, p. 478-484.
[2] Radeş M., *A comparison of some mode indicator functions*, Mechanical Systems and Signal Processing, **8**, 4, 1994, p. 459-474.
[3] Radeş M., *Performance of various mode indicator functions*, Shock and Vibration, **17**, 4-5, 2010, p. 473-482.
[4] Ind P., Robb D., Liu W., Ewins D.J., *Modal testing on the GARTEUR twin*, Proc. Int. Conf. on Structural System Identification, Kassel, Germany, Sept 2001, p. 109-126.
[5] Friswell M., *New measurements on the GARTEUR testbed*, Summary Report, Univ. of Wales Swansea, Dec. 2000.
[6] Breitbach E., *A semi-automatic modal survey test technique for complex aircraft and spacecraft structures*, Proc. 3rd ESRO Testing Symposium, Frascati, Italy, 1973, p. 519-528.
[7] Balmes E., Chapelier C., Lubrina P., Fargette P., *An evaluation of model testing results based on the force appropriation method*, Proc. 13th Int. Modal Analysis Conf., Nashville, Tennessee, 1995, p. 47-53.
[8] Pappa R.S., Elliot K.B., Schenk A., *Consistent mode indicator for the eigensystem realization algorithm*, J. of Guidance, Control and Dynamics, vol. 16, nr. 5, Sept-Oct 1993, p. 852-858.
[9] Radeş M., Ewins D.J., *The aggregate mode indicator function*, Proc. 18th Int. Modal Analysis Conf., San Antonio, Texas, Feb 2000, p. 201-207.
[10] Radeş M., Ewins D.J., *MIFs and MACs in modal analysis*, Proceedings of 20th IMAC Conference on Structural Dynamics, Los Angeles, California, Feb. 2002, p. 771-778.
[11] Shih C.Y., Tsuei Y.G., Allemang R.J. and Brown D.L., *Complex mode indicator function and its application to spatial domain parameter estimation*, Mechanical Systems and Signal Processing, **2**, 4, 1988, p. 367-377.
[12] Hunt D.L., Vold H., Peterson E.L., Williams R., *Optimal selection of excitation methods for enhanced modal testing*, AIAA Paper 84-1068, 1984.
[13] Radeş M., Ewins D.J., *The componentwise mode indicator function*, Proc. 19th Int. Modal Analysis Conf., Kissimmee, Florida, Feb 2001, p. 903-908.